PCCP

PAPER

View Article Online
View Journal | View Issue

Cite this: *Phys. Chem. Chem. Phys.*, 2025, **27**, 8221

Ion dynamics in an iongel electrolyte based on fluorine-free ionic liquid probed by multinuclear NMR†

Andrei Filippov,*[a] Maiia Karlsson-Broström,[a] Rustam Gimatdinov,[b] Faiz Ullah Shah[a] and Oleg N. Antzutkin*[a]

Multinuclear (^{1}H, ^{31}P, and ^{7}Li) NMR was applied to understand the ion dynamics in silica-based iongels with a fluorine-free ionic liquid (IL), tetrabutylphosphonium 2-2-(2-methoxyethoxy)ethoxy acetate, $[P_{4,4,4,4}][MEEA]$, doped with 10 and 30 mol% of LiMEEA. The results were compared with bulk $[P_{4,4,4,4}][MEEA]$/LiMEEA electrolytes and those confined in the "hard" silica matrix of a porous glass. It was found that lithium ion (Li^+) local dynamics and Li^+ diffusion coefficients are strongly affected by confinements in an iongel and in porous glass, as revealed from the analysis of NMR parameters, such as diffusion decays (DDs) in ^{7}Li PFG NMR spectra, broadening of the ^{7}Li NMR resonance lines and variations in the ^{31}P and ^{7}Li chemical shifts. However, NMR diffusometry data do suggest that the studied electrolytes in the iongel confinement have properties like those of bulk electrolytes: (i) high ion diffusivities, (ii) weak alterations of Vogel–Fulcher–Tammann (VFT) parameters for diffusion; and (iii) high transport numbers of ions. The diffusion coefficients of the $[MEEA]^-$ anion and the $[P_{4,4,4,4}]^+$ cation are comparable in the bulk, while they are significantly different in the iongels: the specific interactions of the $[P_{4,4,4,4}]^+$ cations with the negatively charged silica matrix slowed down diffusivities of the cations, while almost no effect of the matrix on diffusivities of the $[MEEA]^-$ anions was noticed. It was also found that the tortuosity of the iongel channels has a negligible effect on diffusivities of ions. The lithium complexation or/and solvation shells of Li^+ ions remained unaffected. Thus, the ionic liquid-based iongel electrolyte acquired the advantages of a semi-solid phase and offered transport properties of a liquid electrolyte.

Received 16th December 2024,
Accepted 23rd March 2025

DOI: 10.1039/d4cp04739g

rsc.li/pccp

Introduction

There is an urge to develop new halogen-free ionic liquids (ILs) for different applications due to their beneficial properties including hydrophobicity, high hydrolytic stability, high thermal and electrochemical stabilities, low melting points and promising ionic conductivities over a wide temperature range.[1–4] ILs may adopt quite complicated supramolecular structures and may have complex ion dynamics. The translational ion dynamics of ILs are related to the structure formed in bulk solutions, near solid surfaces and in confinement. In most electrochemical applications, electrolytes are spatially confined. Therefore, understanding the dynamics of IL-based electrolytes in confinements is of fundamental and practical importance.

Ion mobilities of the confined ILs either increase[5–8] or decrease,[9–13] depending on the nature of the confined space and the chemical structure of the IL. The increase in ionic diffusivities with decreasing pore sizes might allow the development of new applications where high ion mobilities are desired at lower temperatures.[14] A wider practical perspective for confined IL-based electrolytes in the form of iongels (IGs) is available for various energy and environmental applications including supercapacitors, fuel cells and sensors.[15] Typically, IGs are solid or quasi-solid electrolytes based on the trapping of ILs in a silica matrix.[16,17] IG electrolytes have numerous advantages over conventional liquid electrolytes, including less risks of leakage and better mechanical properties.[17] Similar to ILs, IGs offer high thermal stability and electrochemical properties such as ionic conductivity, power density, and an electrochemical stability window.[17–19] The high ionic conductivity and robust mechanical properties of IG electrolytes lead to efficient and flexible energy storage devices for challenging applications.[17]

Molecular level translational mobility in IG electrolyte-based protic ethyl ammonium nitrate (EAN) IL doped with lithium

[a] *Chemistry of Interfaces, Luleå University of Technology, SE-97187 Luleå, Sweden. E-mail: andrei.filippov@ltu.se, Oleg.Antzutkin@ltu.se*
[b] *Department of Physics, Kazan State Medical University, 420012, Kazan, Russian Federation*

† Electronic supplementary information (ESI) available. See DOI: https://doi.org/10.1039/d4cp04739g

nitrate ($LiNO_3$) was studied recently by Parajo *et al.*[20] They showed that the addition of $LiNO_3$ to EAN-IG electrolytes does increase the ionic mobility of the ethyl ammonium cation. Furthermore, the diffusion data revealed the presence of two populations of the ethyl ammonium cation with two different apparent diffusion coefficients. At the same time, Li^+ cations displayed higher mobility in the iongel in comparison with the liquid electrolyte.[20]

Nuclear magnetic resonance (NMR) spectroscopy is a non-invasive method to study molecular interactions and diffusivity in multi-component and multi-phase systems, as well as opaque and porous media.[5,6,9,10,12,21–25] Chemical shifts and multinuclear J-coupling constants are used routinely for the structure elucidation of ILs and the products formed by their covalent-bond interactions with other materials. Pulsed field gradient (PFG) NMR covers a wide range of time extending from milliseconds to seconds and the corresponding length of molecular displacements from sub-micrometers to micrometers. The presence of a host of NMR-active nuclei in ILs permits the widespread use of multinuclear NMR experiments.[6,22,25]

This study is a continuation of our recently reported work,[26] where it was found that the liquid inside the pore ''necks'' and the ''partially isolated volumes'' of the porous glasses stays in a ''slow exchange'' regime with the rest of the (bulk) liquid. The temperature-dependent ion diffusivities in the ''large'' pores deviated from the Arrhenius law and the exchange of diffusing units between the ''narrow'' and the ''large'' pores led to abnormal temperature-dependent diffusion coefficients. Furthermore, the smaller Li^+ diffused more slowly than the larger organic ions in the confinement, demonstrating the solvation of Li^+ inside the pores in the same way as in the bulk. In this work, we analysed ionic interactions and ion dynamics in an iongel electrolyte comprising halogen-free, $[P_{4,4,4,4}]$[MEEA] IL and Li[MEEA] salt with fractions of the salt of 10 and 30 mol% using NMR spectroscopy as well as NMR diffusometry. The IL is composed of tetrabutylphosphonium cations, $[P_{4,4,4,4}]^+$, and 2-[2-(2-methoxyethoxy)ethoxy]-acetate anions, $[MEEA]^-$. The chemical structures and abbreviations of the ionic components of the IL are presented in Fig. 1. The results of the same IL-based electrolyte in bulk and confined in a hard porous glass matrix were assessed for comparison purposes.

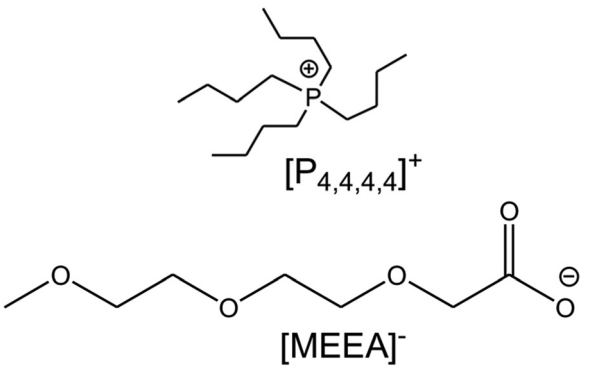

Fig. 1 Chemical structures and abbreviations of the tetrabutylphosphonium cation and the 2-[2-(2-methoxyethoxy)ethoxy]acetate anion of the IL-based iongel electrolyte.

Experimental

Materials and methods

Details of the synthesis and characterisation of the $[P_{4,4,4,4}]$-[MEEA] IL and the LiMEEA salt were previously reported.[27] The silica-based IGs with 10 and 30 mol% of LiMEEA were prepared as described by Negre *et al.*[17] and Parajo *et al.*[20] Briefly, a mixture of 3 mL of ethanol, 0.428 mL of TEOS (tetraethyl orthosilicate 98%, Sigma-Aldrich) and 1 mL of the IL-based electrolyte mixture was prepared in the first step. This mixture was stirred for one hour and then transferred to an appropriate vial and conditioned for 1–2 hours. Then the vial was placed in an oven at 313 K to evaporate the excess of ethanol and to promote a complete gelation after 4 days. Finally, the IG was evacuated under a pressure of 50 Pa for 24 hours to remove residual ethanol and water. While the water content in IL was estimated to be less than 200 ppm,[27] the water content in the IG as estimated by TGA analysis was *ca.* 1 wt% due to the presence of the silica network. The porous glass (PG) confined electrolyte was prepared as described earlier.[26] Varapor100 porous glass (average pore diameter of 9.8 nm) from advanced glass and ceramics (**https://www.porousglass.com**) was used.

NMR techniques

All nuclear magnetic resonance (NMR) experiments were performed using a Bruker Ascend Aeon WB 400 (Bruker BioSpin AG) NMR spectrometer. The working frequencies were 400.21 MHz for ^1H, 162.01 MHz for ^{31}P and 155.56 MHz for ^7Li. All spectra were externally referenced relative to: ^1H resonance (4.7 ppm, water doped with $CuCl_2$), ^7Li resonance (−0.147 ppm, $LiNO_3$ aq.) and ^{31}P (0 ppm, 85% H_3PO_4). Data were processed using Bruker Topspin 3.5 software. For diffusion measurements a Diff50 pulsed-field-gradient (PFG) probe was used. The diffusional decays (DD) were recorded using the stimulated echo (StE) pulse sequence. For single-component diffusion, the form of the DD can be described as:[21]

$$A(\tau, \tau_1, g, \delta) \propto \exp\left(-\frac{2\tau}{T_2} - \frac{\tau_1}{T_1}\right) \exp\left(-\gamma^2\delta^2 g^2 D t_d\right) \qquad (1)$$

Here, A is the integral intensity of the NMR signal, τ and τ_1 are the time intervals in the pulse sequence; γ is the gyromagnetic ratio for magnetic nuclei; g and δ are the amplitude and the duration of the gradient pulse; $t_d = (\Delta - \delta/3)$ is the diffusion time; $\Delta = (\tau + \tau_1)$. D is the diffusion coefficient. In the measurements, δ was in the range of 0.5–3 ms, τ was in the range of 1–3 ms, and g was varied from 0.06 up to 29.73 T m^{-1}. The diffusion time t_d was varied from 20 to 300 ms. The recycle delay during accumulation of signal transients was 3.5 s. Each experiment was repeated at least three times. Non-linear least squares regression was used to fit the experimental data with eqn (1) to extract D values.

To demonstrate the absence of any effect of the internal field gradient directly, a 13-interval stimulated echo sequence with bipolar gradient pulses[28] (Bp2) modified by including a longitudinal Eddy-current-delay[29] was also used. The latter pulse sequence removes cross-terms arising from the applied pulsed

gradients, g and g_0, which are significant even if the g_0 values are small.

Results and discussion

We begin with the assessment of the chemical shifts and resonance line broadening in ^{1}H, ^{31}P and ^{7}Li NMR spectra as a function of temperature and then proceed with the analysis of the ion diffusion data obtained from PFG NMR diffusometry experiments.

NMR spectra

^{1}H NMR spectra of the electrolyte with 30 mol% of LiMEEA in bulk, confined in the porous glass (PG) and in the iongel (IG) are shown in Fig. 2. The ^{1}H NMR spectrum of the bulk electrolyte demonstrates sharp resonance lines for the $[P_{4,4,4,4}]^+$ cation in the range of 0.9–2.4 ppm (the right side of the spectrum), while the resonance lines assigned to protons in the ether groups of $[MEEA]^-$ anions are found to be around 3.2–3.9 ppm (the left side of the spectrum).[27] In comparison, for the electrolyte confined in the pores of the PG, all the ^{1}H NMR resonance lines became broader, and the resolution of the spectrum is much poorer.[26] This is clearly the result of a slower rotational mobility of the ions, resulting in an insufficient averaging of the proton dipole–dipole interactions causing a homogeneous line-broadening.[30] A similar effect is observed in the ^{1}H NMR spectrum of the IG electrolyte. The degree of the ^{1}H resonance line broadening for the IG is comparable with that of the electrolyte confined in the PG.

The ^{31}P NMR and ^{7}Li NMR spectra characterising the $[P_{4,4,4,4}]^+$ cation and the Li^+, respectively, exhibit broad and asymmetric resonance lines with different chemical shifts and line broadening for bulk, PG and IG electrolytes (see Fig. 3). The ^{31}P NMR chemical shifts are different by *ca.* 0.5–1 ppm in these three samples (Fig. 3a) that reflects differences in the electronic environment of $[P_{4,4,4,4}]^+$ cations. The ^{31}P NMR line broadening, while with a "mirror-image" asymmetry (Fig. 3a) is comparable in size in the IG and the PG samples, while both are *ca.* two-fold larger in comparison to the ^{31}P NMR line-width of the cation in the bulk electrolyte. Temperature dependencies of the ^{31}P NMR chemical shifts and the resonance line-widths are shown in Fig. 4a and b, respectively. For all three systems, there is a clear increase in the ^{31}P chemical shift (Fig. 4a) with an increase in temperature that is correlated to the thermal expansion of the samples. Interestingly, the slopes of the "chemical-shifts *vs.* temperature" curves are comparable for all three samples, probably due to similarities in variations of local compositions of the electrolyte in bulk and the confinements. The ^{31}P resonance line broadening, ΔH, does not depend on temperature for the bulk sample (Fig. 4b, black circles), suggesting a rather free rotational mobility of the phosphonium cation in the whole temperature range.

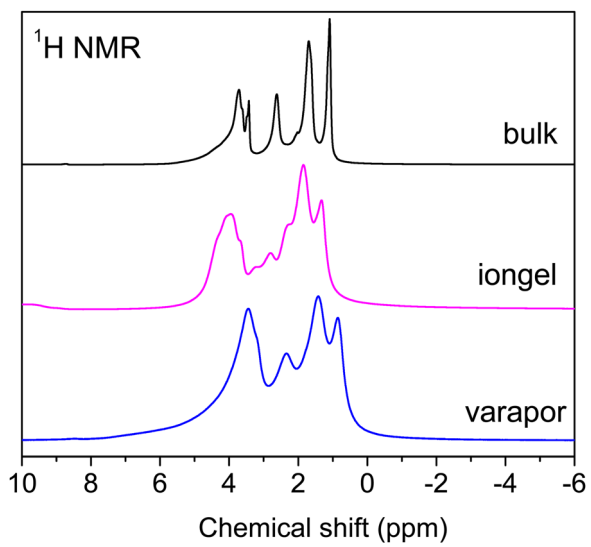

Fig. 2 ^{1}H NMR spectra of the bulk, confined in Varapor PG and IG-based $[P_{4,4,4,4}][MEEA]$ electrolytes (30 mol% of LiMEEA) at 295 K.

For the electrolyte confined in PG (red circles), the ΔH is twice larger at low temperatures in comparison with the bulk. There is a sharp decrease in the linewidth (by a factor 1.8) as the temperature increases, which agrees with the change in regime of diffusion of the electrolyte in this system:[26] heating of the sample up to ~330 K leads to intensifying of the exchange of the electrolyte between "small" and "large" pores of Varapor's pore size distribution. For the IG sample (green circles) ΔH is also almost twice larger in comparison to the bulk. The temperature dependence of ΔH in the iongel is weaker than that in PG, while a slight decrease (by a factor ~1.1) in the line width with an increase in temperature is also perceived, and the decrease proceeds monotonously in the whole temperature range. This suggests that there is not a sharp transition between the motional regimes for the cation in the IG and reflects a difference in the structures of networks of pores in these two samples (PG *vs.* IG). Varapor has a "hard" structure of a porous silica matrix: its thermal expansion leads to a variation in the structure of pores and interpore connections.

The ion dynamics inside the pores and between the pores follows the pore structure alteration. Therefore, variation in the matrix structure of PG with temperature is an important factor for ion electrolyte dynamics in the confinement. On the other hand, the silica matrix of the IG is "soft"; and therefore, in contrast to the matrix of the PG, is controlled by the ion dynamics of a confined electrolyte. It is also interesting to notice that the values of ΔH in IG are smaller than the ΔH values in Varapor at temperatures below 330 K, and larger than in the PG at temperatures above 330 K. The thermal expansion of the PG matrix together with the thermal activation of the cations liberates reorientational mobility of the cations at $T > 330$ K. In contrary, the IG silica network filled with the electrolyte monotonously expands with an increase in temperature in the measured interval from 295 to 365 K.

The ^{7}Li NMR chemical shifts and line-widths for the electrolyte in the bulk and confinements are shown in Fig. 5a and b, respectively. The change in ^{7}L NMR chemical shifts for different samples (Fig. 5a) follow the same trend as for the ^{31}P NMR

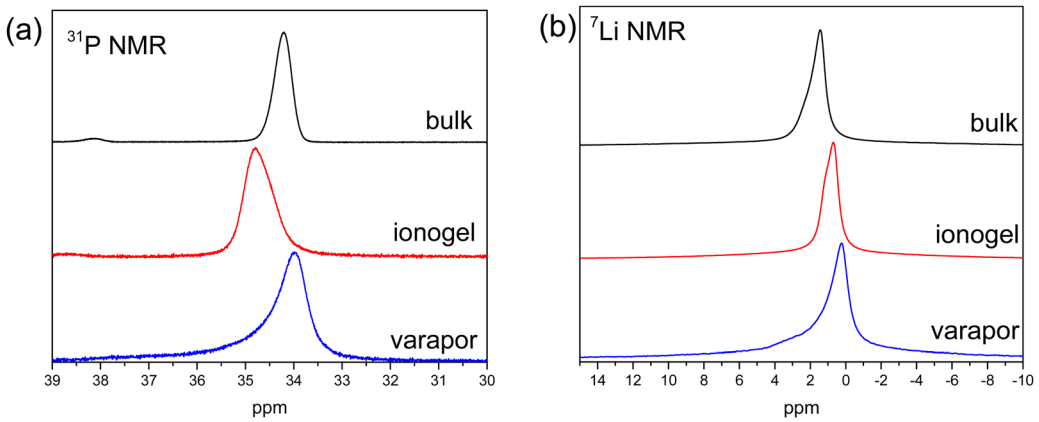

Fig. 3 ^{31}P (a) and ^{7}Li (b) NMR spectra of the electrolyte ([$P_{4,4,4,4}$][MEEA] with 30 mol% of LiMEEA) in the bulk, pores of PG and in IG. T = 295 K.

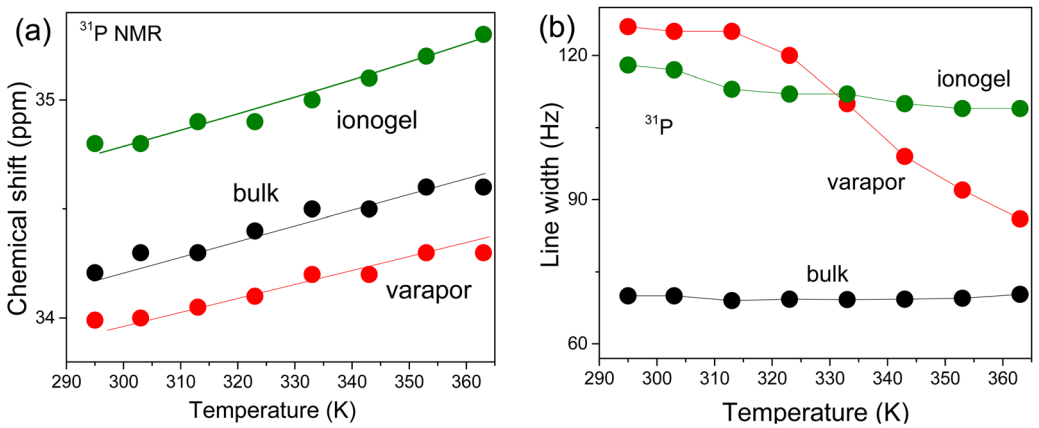

Fig. 4 Temperature dependences of ^{31}P NMR chemical shifts (a) and resonance line-widths (b) for the bulk and confined ([$P_{4,4,4,4}$][MEEA] with 30 mol% LiMEEA) electrolyte: bulk (black circles), Varapor (red circles) and iongel (green circles).

chemical shifts (Fig. 4a): δ (iongel) > δ (bulk) > δ (Varapor). There is almost no significant change in the ^{7}Li chemical shifts with an increase in temperature in all three systems. This might be because the Li^+ cations persist in a highly bound state due to their solvation shells inside the electrolytes. The bound state of the Li^+ is seen also from its much lower diffusivity in comparison with other liquid components of the electrolyte.[26] The ^{7}Li line widths demonstrate an increase in the degree of restriction of mobility of Li^+ from the bulk to IG and further to PG (Fig. 5b). It seems to be that there is no any visible transition between

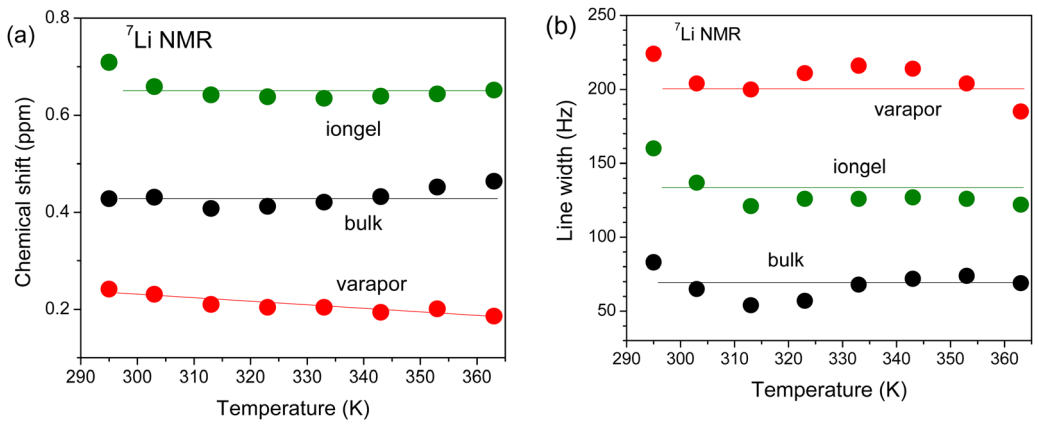

Fig. 5 Temperature dependences of the ^{7}Li NMR chemical shift (δ) (a) and resonance line-widths (b) for the bulk (black circles) and those confined in PG (red circles) and IG ([$P_{4,4,4,4}$][MEEA] with 30 mol% LiMEEA) electrolyte.

regimes of mobility for Li^+ in contrast to the clear transition in mobility for the $[P_{4,4,4,4}]^+$ cation in Varapor at 330 K (see Fig. 4b). This can also be a consequence of the bound state of Li^+, for which the thermal expansion of the Varapor silica matrix does not open enough space to perform the transition.

Ion diffusivity

The diffusion decays (DDs) of ^1H NMR, ^{31}P and ^7Li resonances of the bulk electrolyte are in the form of a single-component diffusion (eqn (1)), as reported earlier.[26] The diffusion coefficients of the organic ions are comparable to each other, while diffusivity of the Li^+ ions is a factor 1.7–3.7 less than those of the organic anions and cations. For the electrolyte confined in pores of the PG, the ^1H and ^{31}P DDs have no-single-component forms, which additionally depend on the temperature, while the ^7Li DDs have a clear singe-component form.[26] Diffusivity of the $[P_{4,4,4,4}]^+$ cations demonstrates a complicated dependence with an increase in temperature, and diffusivity of the Li^+ cations further decreases when compared to that in the bulk.

The ^1H, ^{31}P and ^7Li for the electrolyte confined in IGs was measured by the PFG NMR stimulated echo method. The typical ^1H DDs for the bulk and confined electrolyte are shown in Fig. S1 in the ESI.† It is seen that ^1H DDs for the IG sample deviate from the single-component form in the third decimal order of the signal decay that demonstrates a distribution of diffusion coefficients in the confinement, which is not as broad as in the case of the electrolyte confined in the PG. However, in two decimal orders of the signal decay, the DDs are comparable to the single-component form (Fig. S2 in the ESI†), and do not show any distinct dependence on the diffusion time (Fig. S3 in the ESI†). The same was observed for diffusion of the cation (Fig. S4 in the ESI†) as well as Li^+ (Fig. S5 in the ESI†).

The temperature dependent diffusion coefficients of the electrolyte confined in the IG are shown in Fig. 6, alongside those of the bulk and the PG-confined electrolyte. The diffusion coefficients obtained for the anion (green circles) are like those in the bulk throughout the studied temperature range. The diffusion coefficients of the cation (green triangles) are lower in comparison with the bulk (black triangles) and the difference increases as the temperature increases up to the factor of 1.4 at 363 K. At the same time, the degree of decrease of diffusion coefficients of the organic cation in the IG is smaller than that in PG (red triangles). The diffusivity of the Li^+ in IG (green stars) is also slower compared to the bulk (by a factor 1.15) but is higher in comparison with Li^+ diffusivity in the PG (red stars). Generally, ion diffusivities of the electrolyte in the IG are in between of those of bulk and confined in the PG. There is no deviation as previously observed for diffusivity of anions in the Varapor-confined electrolyte in the high temperature range (open red circles),[26] evidently because of the "soft" structure of the IG silica matrix and its gradual swelling upon heating.

In the case of the electrolyte confined in the IG, the form of DDs is close to the single-exponential function, which means that at the time (less than 20 ms) and in the corresponding spatial scale of the NMR PFG experiment (less than 1 μm) almost complete averaging occurs due to diffusion of the ions. There is no bi-exponential DDs observed as observed earlier for IG based ethyl ammonium nitrate (EAN).[20] There is no "hidden" protons present in the system under study (as in EAN and other protic ILs). These protons are not detected by spin-echo NMR due to their fast T_2 relaxation rates but can influence the dynamic parameters (relaxation and NMR diffusion) of other (visible) protons through exchange. This could lead to a distortion of the temperature dependence due to the exchange of protons between cations and anions. In Fig. 6, it is seen that diffusivities of the anions exceed the diffusivities of the cations (green triangles) by a factor of ~1.2–2.2, and the difference in the diffusivities increases as the temperature increases. Based on this difference, like the case of the PG in the low-temperature range, it can be concluded that confinement of the IG leads to a decrease in diffusivities of cations relative to that in bulk, while diffusivities of the $[MEEA]^-$ anions remain comparable to those in the bulk. The temperature dependence of Li^+ diffusion coefficients is shown in Fig. 6 as green stars, which demonstrates a convex form like bulk and the PG-contained electrolyte. However, diffusivities of the Li^+ are a factor of 1.2–1.4 smaller than those of the bulk electrolyte.

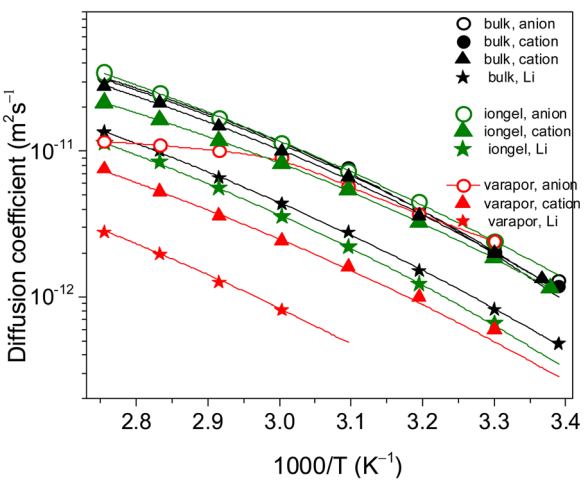

Fig. 6 Temperature dependences of diffusion coefficients obtained by ^1H (circles), ^{31}P (triangles) and ^7Li (stars) PFG NMR stimulated echo experiments for the electrolyte (30 mol% of LiMEEA) in bulk (black), in pores of Varapor (red) and in IG (green). Temperature dependences for the bulk and the Varapor-confined electrolyte were previously published.[26]

The temperature-dependent diffusion coefficients of the ions for bulk and IG-confined electrolyte with 10 mol% of LiMEEA are shown in Fig. S6 and S7 in the ESI.† The dependences of ion diffusivities have convex forms like for the electrolyte with 30 mol% of the salt (Fig. 6). As expected, the increase of lithium salt concentration in the bulk leads to a decrease in the diffusivities of all ions. Furthermore, confinement of the electrolyte with 10 mol% of the salt in IG resulted in decreased diffusivities of the ions.

This study confirms that IG preserves the liquid-like behaviour of the IL-based electrolyte upon confinement.[17,20] The confinement of the IL-based electrolyte in IGs has some similarities to the confinement in the pores of the PG: (1) the

diffusivities of organic ions demonstrate multi-component characteristics, which can be formally characterised as the spectra of apparent diffusion coefficients; (2) the diffusivity of the cations decreases at a higher degree compared with those of the anions; (3) the diffusivity of Li^+ shows a single-component diffusion similar to the bulk and decreases in confinements. On the other hand, the effect of confinement in IG is very 'delicate' in comparison with the confinement in the 9.8 nm "hard" porous structure of the PG: (1) the degree of decrease in the diffusivities of the cation and Li^+ in IG are minor; (2) there are no "small" pores in the IG, where enhancement in ^{1}H NMR transverse relaxation prevents measurements of the diffusivity for a part of the ions.[26] (3) Averaging of the diffusivities over the system in the case of IG occurs over the time and spatial scale attainable to the PFG NMR experiment.

It is known that the silica and silicate glass surfaces acquire a negative surface charge density due to deprotonation of –OH chemical groups.[31] Therefore, interaction of the $[P_{4,4,4,4}]^+$ cation with the negative surface might be a possible mechanism of the stronger decrease in translational diffusion as compared with the $[MEEA]^-$ anions. It is already well known that Li^+ ions diffuse much slower in IL-based electrolytes,[2,4,18,20,27] which is proposed to be due to the formation of lithium complexes or the formation of solvation shells near the Li^+ ions. It was observed for the EAN-based electrolyte[20] that confinement in narrow pores of PGs and IG could destabilise these complexes and enhance the diffusivity of lithium. This study confirms that the dynamics of Li^+ is strongly linked to gelation, however, we did not observe any signs of breaking the lithium complexes in our system. It could be proposed that the lithium salt concentration in the electrolyte with 30 mol% of the salt is too high. However, as shown (Fig. S6 in the ESI†), the diffusivities of all ions in the bulk at 10 mol% of the salt are much higher than those in the electrolyte containing 30 mol% of the salt. Confining the 10 mol% containing LiMEEA in the IG leads to decreased diffusivities of all the ions, including Li^+ (Fig. S7 in the ESI†). Therefore, confining of the electrolyte in the IG matrix does not break down the lithium complexes in the case of our electrolytes.

The diffusivities as a function of temperature for all the ions confined in IG, as well as in the bulk and in the PG (with the exception of $[MEEA]^-$ anions in Varapor) demonstrated a convex form, typical for bulk electrolyte ions. To further analyse such dependences, we employed a Vogel–Fulcher–Tammann (VFT) empirical approach widely used as a convenient tool for systems with a characteristic liquid-glass transition.[32–34] The VFT model in the case of ion diffusivity has a form[35] with three adjustable parameters, D_0, T_0 and E_D:

$$D = D_0 \exp\left(\frac{-E_D}{R(T - T_0)}\right) \quad (5)$$

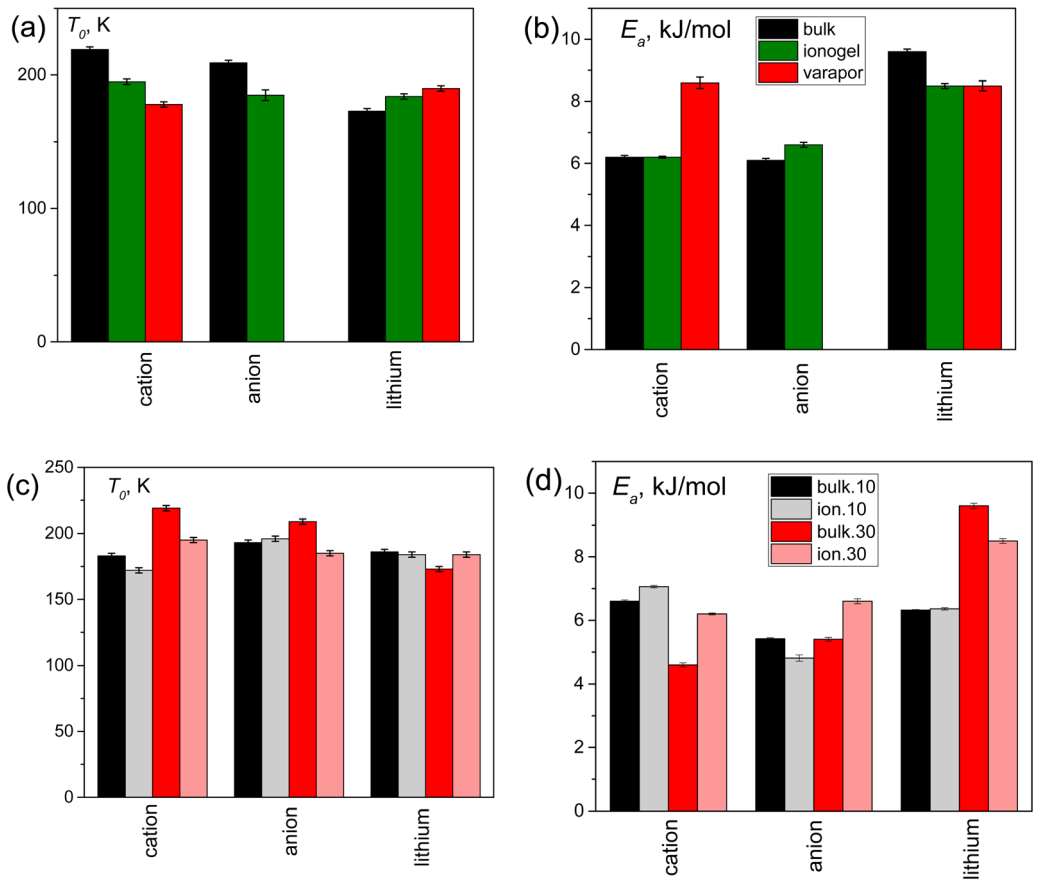

Fig. 7 Parameters of the VFT fitting for temperature-dependent diffusion coefficients of the ions. The values are tabulated in Fig. 6 and Fig. S7 (ESI†).

where D_0 is a pre-exponential factor, T_0 is the so-called "Vogel temperature" or "ideal glass transition temperature". T_0 is related directly to the fluctuations of the bond strength and the coordination number of the structural units.[33] E_D is the apparent activation energy for diffusion, and R is the gas constant. Values of D_0, T_0 and E_D obtained from the temperature dependences of diffusivities for electrolytes with 30 mol% and 10 mol% of LiMEEA (Fig. 6 and Fig. S7, ESI†) in such analyses are presented in Tables S1 and S2 in the ESI.† For comparison, these parameters are also presented in Fig. 7.

Though the VFT analysis is quite formal, we can see certain trends (in the increase of degree of constraint in the order bulk → IG → PG), which characterise alteration of parameters of the translational ion dynamics. This order of degree of constrains for ion diffusivity is also seen from the degree of decrease in the ion diffusion coefficients (Fig. 6) and the degree of non-exponentiality of ^{1}H DDs (Fig. S1, ESI†). T_0 (Fig. 7a and c) shows a weak trend of decreasing with the increase in the degree of constraints for the organic cations and anions, while with the opposite trend is seen for the Li^+. The apparent activation energy for ion diffusion (Fig. 7b and d) shows a weak trend of increasing for the organic cations and anions, but E_D slightly decreases for the Li^+. Generally, the decrease of T_0 and the increase of E_D with an increase in the degree of restriction agrees with a common understanding of the effects of constraints, which leads to retardation of the diffusion process. This can be related to the peculiarity of associated states of the Li^+ in bulk of the ionic liquid systems,[36] which can be additionally modified in the presence of negatively charged silica. While for EAN-based electrolytes it was shown that rotational and translational mobilities of Li^+ increase upon confinement in silica-based IGs,[20] in our study, an opposite effect is clearly observed. The increase in the ^{7}Li NMR spectral linewidth and the decrease in Li^+ diffusion coefficients with increasing degree of constraints from the bulk to the IG and further to PG, highlight the remarkable stability of the lithium complexes in these systems.

Effect of tortuosity on the ion diffusivity

The decrease in ion diffusivity in confinement can be related with the interactions between molecules and ions of interest and the confining matrix because of adsorption, precipitation and changing in structures of the molecular/ionic assemblies. Another mechanism, which might lead to a decrease in the molecular/ionic diffusivity is a complexity of the percolation paths in the interconnected system of channels. This effect is usually expressed as tortuosity, which reflects the efficiency of percolation paths and is linked to the topology of the material.[37] Tortuosity, understood as a topologic characteristic of the porous network independent of the used probe. One of the methods to evaluate tortuosity is the determination of the ratio between the value of the diffusion coefficient of a probe in the bulk to its apparent value in the porous network. It is important that the probe molecule/ion is displaced at a distance much longer than the characteristic scale length of the porous matrix: long-term diffusion, the root-mean-square displacements of molecules are larger than the correlation length of the porous space ξ, and the motion of liquid molecules is averaged over the space of the system,[38,39] giving exponential DD and diffusion time independent diffusion coefficient $D^* = D_\infty$. In a well-connected porous medium, D^* approaches at long times a finite value, which can be expressed through tortuosity α:[38]

$$D^* \sim D_0/\alpha \quad (6)$$

Our previous evaluations gave tortuosities of Varapor PG of ~2.94 for both ethylammonium nitrate ionic liquid and non-ionic *n*-decane.[9] Regarding the IG-confined electrolytes used in this study: there is no diffusion-time dependence of the ion diffusion coefficients (Fig. S3, ESI†) that corresponds to the long-term diffusion. The diffusivity of one selected ion, the $[MEEA]^-$ anion, which is less prone to interact with the silica matrix, is comparable to that in the bulk (Fig. 6 and Fig. S7, ESI†). This demonstrates that the effect of tortuosity on ions confined in the IG is negligible, that is $\alpha \sim 1$. On the other hand, keeping in mind no-dependence of tortuosity on the probe molecule/ion, the decrease in the diffusivities of $[P_{4,4,4,4}]^+$ and Li^+ in the IG is obviously conditioned by their specific interactions with the IG silica matrix.

Transport numbers

The transport number is defined as the ratio of the electric current derived from the cation to the total electric current. The transport numbers (t_i) for each ion in the electrolytes can be calculated from their diffusion coefficients using eqn (7):[40,41]

$$t_i = \frac{x_i D_i}{\sum_i x_i D_i} \quad (7)$$

where x_i is the molar fraction of each ion. Results of calculations of t_i for the bulk and IG-confined electrolyte are shown in Fig. 8.

The $[MEEA]^-$ anions exhibit higher transport numbers in both electrolytes as compared to the $[P_{4,4,4,4}]^+$ and Li^+, and this is obviously due to the higher content of the $[MEEA]^-$ anions in these systems (Fig. 8). The t_i of Li^+ is the smallest due to two main reasons: the lower Li^+ concentration and the potential aggregate formation facilitated by the Li^+. It is also well known that transport numbers obtained from PFG NMR diffusometry are underestimated due to aggregate formation in electrolytes and do not reflect the true ionic contributions to conductivity, and the values are often approximately half of those determined by electrochemical techniques.[41]

Diffusivity of water

Since ethanol was used in preparation of the iongel samples and even though ethanol was evaporated under high vacuum, there can still be traces of trapped water in the hydrophobic silica matrix. In porous glasses, there is no such water because of the thermal activation of glasses at 450 °C before their saturation with the electrolyte. However, the trapped water present in IG leads to a broadening of the ^{1}H NMR spectrum line in the range of 3.5–4.5 ppm (Fig. 2). Application of a spin-

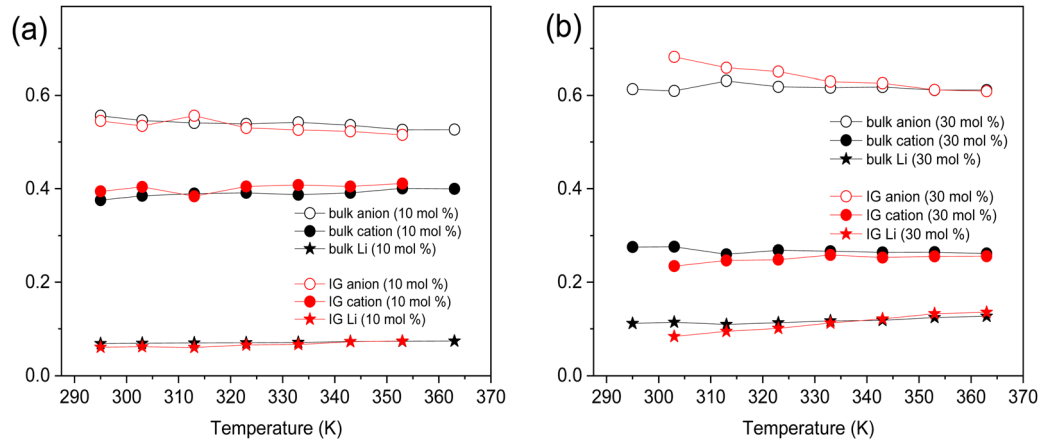

Fig. 8 Transport numbers for ions in the bulk and IG-confined electrolytes at 10 mol% (a) and 30 mol% (b) LiMEEA in the temperature range 293–363 K calculated using eqn (7) and diffusivities of ions from Fig. 6 and Fig. S7 (ESI†).

echo pulse sequence can effectively increase the water apparent fraction in diffusion decays (eqn (1)) due to slower NMR relaxation of water's protons. In our experiments, the ^{1}H NMR diffusion decay of water was separated from the entire diffusion decay as its contribution in the ^{1}H NMR chemical shift is in the range of 3.5–4.5 ppm having the activation energy for diffusion (E_D) comparable to the E_D of bulk water, $\sim$18 kJ mol^{-1} (Fig. S8 in the ESI†). This value of the E_D is significantly different from the activation energies of the ionic components in bulk and confinements (Fig. 7b and d). As is clear, water trapped in the IG has a higher diffusivity than other molecules/ions, but lower than that of the bulk water. The presence of water signals should be taken into consideration while analysing the diffusivity of the other components confined in IG, particularly the anions. Similar maintenance of the activation energy of diffusion for a fluid after confinement in nanopores was observed earlier for ethyl ammonium nitrate (EAN) in the pores of PGs.[9]

Conclusions

This multinuclear (^{1}H, ^{31}P and ^{7}Li) NMR study revealed that the iongel electrolyte preserves liquid-like beneficial transport properties such as faster ion diffusivities, a weak alteration of the apparent activation energy for diffusion and comparable transport numbers to liquid electrolyte. Although ions of the bulk electrolyte showed a single-component diffusional behaviour, some distribution of the apparent diffusion coefficients is observed for the organic ions in the iongel. The specific interactions of cations with the negatively charged silica matrix decreased diffusivity of the cation, while the diffusivity of the anion remained unaffected. The dynamic glass transition temperature and apparent activation energies for ion diffusion remained unchanged with increasing of the molar fraction of Li[MEEA] in the ionic liquid based [$P_{4,4,4,4}$][MEEA] electrolyte. The local dynamics and diffusivity of the Li^{+} are strongly affected inside the porous glass and in the iongel, however, the aggregates/complexes of lithium remained stable in the studied temperature range, as confirmed by ^{7}Li NMR spectroscopy. This study provides insights into a fluorine-free IL-based iongel that can potentially be used as a safer lithium battery electrolyte.

Author contributions

A. F.: conceptualization, methodology, preparation of iongels, and writing – original draft; O. N. A.: validation, reviewing and editing; M. K.-B.: NMR diffusion experiment and data curation; R.G.: diffusion data analysis; and F. U. S.: validation, reviewing and editing.

Data availability

The data supporting this article have been included in the ESI.†

Conflicts of interest

The authors declare that they have no known competing financial interests or personal relationship that could have appeared to influence the work reported in this paper.

Acknowledgements

The financial support from the Swedish Research Council for Sustainable Development (Grant number: 2020-00969) and the European Regional Development Fund (Interreg Aurora, project number: 20366551) are gratefully acknowledged. We are grateful to the Foundation in memory of J. C. and Seth M. Kempe for the NMR equipment grants.

References

1 F. U. Shah, S. Glavatskih, D. R. MacFarlane, A. Somers, M. Forsyth and O. N. Antzutkin, *Phys. Chem. Chem. Phys.*, 2011, **13**, 12865–12873.
2 S. Bhowmick, G. Tatrari, A. Filippov, P. Johansson and F. U. Shah, *Phys. Chem. Chem. Phys.*, 2023, **25**, 19815–19823.

3 A. B. Reddy, F. U. Shah, J. Leckner, M. W. Rutland and S. Glavatskih, *Colloids Surf., A*, 2024, **683**, 132875.
4 M. Ahmed, S. Rao, A. Filippov, P. Johansson and F. U. Shah, *Phys. Chem. Chem. Phys.*, 2023, **25**, 3502–3512.
5 A. Filippov, N. Azancheev, F. U. Shah, S. Glavatskih and O. N. Antzutkin, *Micropor. Mesopor. Mater.*, 2016, **230**, 128–134.
6 C. Iacob, J. R. Sangoro, W. K. Kipnusu, R. Valiullin, J. Kärger and F. Kremer, *Soft Matter*, 2012, **8**, 289–293.
7 C. Pinilla, M. G. Del Popolo, R. M. Lynden-Bell and J. Kohanoff, *J. Phys. Chem. B*, 2005, **109**, 17922–17927.
8 Q. Berrod, F. Ferdeghini, P. Judenstein, N. Genevaz, R. Ramos, A. Fournier, J. Dijon, J. Olliver, S. Rols, D. Yu, R. A. Moled and J.-M. Zanotti, *Nanoscale*, 2016, **8**, 7845–7848.
9 A. Filippov, O. N. Antzutkin, V. P. Arkhipov and O. I. Gnezdilov, *J. Mol. Liq.*, 2022, **356**, 118998.
10 Y. Wei, Z. Dai, Y. Dong, A. Filippov, X. Ji, A. Laaksonen, F. U. Shah, R. An and H. Fuchs, *Phys. Chem. Chem. Phys.*, 2022, **24**, 12808–12815.
11 S. Zhang, J. Zhang, Y. Zhang and Y. Deng, *Chem. Rev.*, 2017, **117**, 6755–6833.
12 C. Iacob, J. R. Sangoro, P. Papadopoulus, T. Schubert, S. Naumov, R. Valiullin, J. Kärger and F. Kremer, *Phys. Chem. Chem. Phys.*, 2010, **12**, 13798–13803.
13 E. H. Lahrar, I. Deroche, C. M. Ghimbeu, P. Simon and C. Merlet, *ACS Appl. Nano Mater.*, 2021, **4**, 4007–4015.
14 H. Frielinghaus, M. Fomina, D. Hayward, P. S. Dubey, S. Jaksch, P. Falus, P. Fouquet, L. Fruhner and O. Holderer, *Front. Phys.*, 2022, **10**, 872616.
15 M. P. Singh, R. K. Singh and S. Chandra, *Prog. Mater. Sci.*, 2014, **64**, 73–120.
16 M. Brachet, T. Brousse and J. Le Bideau, *ECS Electrochem. Lett.*, 2014, **3**, A112–A115.
17 L. Negre, B. Daffos, V. Turq, P. L. Taberna and P. Simon, *Electrochim. Acta*, 2016, **206**, 490–495.
18 S. A. M. Noor, P. M. Bayley, M. Forsyth and D. R. MacFarlane, *Electrochim. Acta*, 2013, **91**, 219–226.
19 I. H. Sajid, M. F. M. Sabri, S. M. Said, M. F. M. Salleh, N. N. N. Ghazali, R. Saidur, B. Subramaniam, S. W. Hasan and H. A. Jaffery, *Energy Convers. Manag.*, 2019, **198**, 111813.
20 J. J. Parajó, P. Vallet, M. Villanueva, O. Cabeza, F. Fernández-Carretero, A. García Luis, M. E. Di Pietro, A. Mele, F. Castiglione, J. Salgado and L. M. Varela, *J. Mol. Liq.*, 2024, **397**, 124093.
21 P. T. Callaghan, *Principles of Nuclear Magnetic Resonance Microscopy*, Clarendon, Oxford, 1991.
22 V. Overbeck, A. Appelhagen, R. Rößler, T. Niemann and R. Ludwig, *J. Mol. Liq.*, 2021, **322**, 114983.
23 G. Ori, F. Villemot, L. Viau, A. Vioux and B. Coasne, *Mol. Phys.*, 2014, **112**, 1350–1361.
24 P. Linse and O. Söderman, *J. Magn. Reson., Ser. A*, 1995, **116**, 77–86.
25 K. Damodaran, *Progr. Nucl. Magn. Reson. Spec.*, 2022, **129**, 1–27.
26 A. Filippov, M. Rudakova, V. P. Archipov and F. U. Shah, *Soft Matter*, 2024, **20**, 8436–8445.
27 F. U. Shah, O. I. Gnezdilov, I. A. Khan, A. Filippov, N. A. Slad and P. Johansson, *J. Phys. Chem. B*, 2020, **124**, 9690–9700.
28 R. M. Cotts, M. J. R. Hoch, T. Sun and J. T. Markert, *J. Magn. Reson.*, 1989, **83**, 252–266.
29 S. J. Gibbs and C. S. JohnsonJr, *J. Magn. Reson.*, 1991, **93**, 395–402.
30 M. Levitt, *Spin Dynamics: Basics of Nuclear Magnetic Resonance*, 2nd edn, Wiley, Chichester, 2008.
31 S. H. Behrens and D. G. Grier, *J. Chem. Phys.*, 2001, **115**, 6716–6721.
32 P. G. Debenedetti and F. H. Stillinger, *Nature*, 2001, **410**, 259–267.
33 M. Ikeda and M. Aniya, *J. Non-Crystal Solids*, 2013, **371–372**, 53–57.
34 E. M. Morais, A. Idström, L. Evenäs and A. Martinelli, *Molecules*, 2023, **28**, 5147.
35 H. Tokuda, K. Hayamizu, K. Ishii, M. A. B. H. Susan and M. Watanabe, *J. Phys. Chem. B*, 2005, **109**, 6103–6110.
36 M. Brinkkötter, A. Mariani, S. Jeong, S. Passerini and M. Schönhoff, *Adv. Energy Sustainability Res.*, 2020, **1**, 2000078.
37 M. Barrande, R. Bouchet and R. Denoyel, *Anal. Chem.*, 2007, **79**, 9115–9121.
38 P. N. Sen, *Concepts Magn. Reson. A*, 2004, **23A**, 1–21.
39 V. Skirda, A. Filippov, A. Sagidullin, A. Mutina, R. Archipov and G. Pimenov, in Fluid Transport in Nanoporous Materials, *Book series: NATO Science Series II-Mathematics Physics and Chemistry*, 2006, 219, 255–278.
40 T. Fromling, M. Kunze, M. Schonhoff, J. Sundermeyer and B. Roling, *J. Phys. Chem. B*, 2008, **112**, 12985–12990.
41 M. Gouverneur, J. Kopp, L. Van Wüllen and M. Schönhoff, *Phys. Chem. Chem. Phys.*, 2015, **17**, 30680–30686.